EMILIN1–α4/α9 integrin interaction inhibits dermal fibroblast and keratinocyte proliferation

Carla Danussi,[1] Alessandra Petrucco,[1] Bruna Wassermann,[1] Eliana Pivetta,[1] Teresa Maria Elisa Modica,[1] Lisa Del Bel Belluz,[1] Alfonso Colombatti,[1,2,3] and Paola Spessotto[1]

[1]Division of Experimental Oncology 2, Centro di Riferimento Oncologico, Istituto di Ricovero e Cura a Carattere Scientifico, National Cancer Institute, 33081 Aviano, Italy
[2]Department of Biomedical Science and Technology and [3]Microgravity, Ageing, Training, and Immobility Excellence Center, University of Udine, 33100 Udine, Italy

EMILIN1 promotes α4β1 integrin–dependent cell adhesion and migration and reduces pro–transforming growth factor–β processing. A knockout mouse model was used to unravel EMILIN1 functions in skin where the protein was abundantly expressed in the dermal stroma and where EMILIN1-positive fibrils reached the basal keratinocyte layer. Loss of EMILIN1 caused dermal and epidermal hyperproliferation and accelerated wound closure. We identified the direct engagement of EMILIN1 to α4β1 and α9β1 integrins as the mechanism underlying the homeostatic role exerted by EMILIN1. The lack of EMILIN1–α4/α9 integrin interaction was accompanied by activation of PI3K/Akt and Erk1/2 pathways as a result of the reduction of PTEN. The downregulation of PTEN empowered Erk1/2 phosphorylation that in turn inhibited Smad2 signaling by phosphorylation of residues Ser245/250/255. These results highlight the important regulatory role of an extracellular matrix component in skin proliferation. In addition, EMILIN1 is identified as a novel ligand for keratinocyte α9β1 integrin, suggesting prospective roles for this receptor–ligand pair in skin homeostasis.

Introduction

The skin is composed of an epithelial and a mesenchymal compartment (Fuchs and Raghavan, 2002). The hallmark of the epidermis is its ability to self-renew throughout the entire life span of the organism (Clayton et al., 2007; Blanpain and Fuchs, 2009). The mouse skin epidermis maintains a single basal layer of proliferating cells, which adhere to an underlying basement membrane (BM) rich in ECM proteins, proteoglycans, and growth factors. Basal cells receive microenvironmental cues influencing proliferation or differentiation and rely on both mesenchymal cell stimuli and the ECM (Fuchs, 2007; Blanpain and Fuchs, 2009). An important and still unanswered question is how the surrounding microenvironment and, in particular, the ECM constituents influence basal keratinocyte and dermis fibroblast behavior during normal homeostasis.

The cell integrins and their ECM ligands provide a diverse repertoire of proliferative stimuli for skin basal cells and are key regulators of keratinocyte growth control (Singer and Clark, 1999; Watt, 2002). Basal keratinocytes express several integrins at the basolateral pole: α3β1, the laminin-5 receptor; α2β1, the collagen receptor that likely mediates cell–cell interactions; α5β1, the fibronectin receptor; and αvβ3 and αvβ6, the vitronectin receptors (Watt, 2002; Owens and Watt, 2003). Finally, integrin α9β1, normally expressed only in the basal layer (Palmer et al., 1993; Stepp et al., 2002), has several ECM ligands that are prominently expressed beneath migrating keratinocytes only during wound healing (Yokosaki et al., 1994, 1996; Liao et al., 2002; Shinde et al., 2008). Among these, tenascin-C and the EIIIA segment of fibronectin are barely expressed under nonpathological conditions (Singh et al., 2004), suggesting that other ligands may bind to α9β1 at the dermal–epidermal junction in normal conditions.

EMILIN1 (elastic microfibril interface–located protein 1) is an ECM multidomain glycoprotein associated with elastic fibers (Colombatti et al., 1985; Bressan et al., 1993) particularly abundant in the walls of large blood vessels (Zanetti et al., 2004) in intestine, lung, lymph nodes, skin, and lymphatic capillaries (Danussi et al., 2008). This glycoprotein is characterized by a

Correspondence to Alfonso Colombatti: acolombatti@cro.it

Abbreviations used in this paper: BM, basement membrane; CAFCA, centrifugal assay for fluorescence-based cell adhesion; CK, cytokeratin; H/E, hematoxylin/eosin; HF, hair follicle; NIH, National Institutes of Health; RD, rhabdomyosarcoma; shRNA, short hairpin RNA; WT, wild type.

The Rockefeller University Press $30.00
J. Cell Biol. Vol. 195 No. 1 131–145
www.jcb.org/cgi/doi/10.1083/jcb.201008013

region homologous to the globular domain of C1q (gC1q domain) at the C-terminal end (Doliana et al., 1999; Colombatti et al., 2000) involved in EMILIN1 oligomerization (Mongiat et al., 2000), cell adhesion, migration, and trophoblast invasion via interaction with the α4β1 integrin (Spessotto et al., 2003, 2006). The hallmark of the EMILIN family is the elastin microfibril interface domain at the N terminus (Doliana et al., 2000), which interacts with pro–TGF-β (Zacchigna et al., 2006). EMILIN1 has been implicated in multiple functions, including elastogenesis, maintenance of blood vascular cell morphology (Zanetti et al., 2004), and regulation of the growth and integrity of lymphatic vessels (Danussi et al., 2008). *Emilin1*$^{-/-}$ mice display elevated blood pressure as a result of increased TGF-β signaling in the vasculature (Zacchigna et al., 2006). These mice also have an abnormal lymphatic phenotype with a significant reduction of anchoring filaments and lymphatic vessel hyperplasia, leading to a mild lymphatic dysfunction (Danussi et al., 2008).

Here, we report that *Emilin1*$^{-/-}$ mice present dermal and epidermal hyperproliferation and indicate that EMILIN1 negatively regulates cell growth. Our findings support a model in which EMILIN1 interacts with α4β1 or α9β1 integrin to provide an important external cue for the maintenance of a correct skin homeostasis.

Results

EMILIN1 produced by dermal fibroblasts contacts basal keratinocytes

EMILIN1 was highly expressed as a network in the dermis stroma, whereas it was absent in the epidermis. Interestingly, we noticed some EMILIN1-positive fibrils departing from the region below the basal membrane and reaching up to basal keratinocytes (Fig. 1, A and B). EMILIN1 also was particularly abundant in the outer root sheath of the hair follicle (HF) forming a basket-shaped network around the hair bulb and displayed protrusions toward the keratinocytes in the follicle bulb (Fig. 1 C).

The peculiar localization of EMILIN1 up to the basal layer of keratinocytes raised the question as to whether it was synthesized and deposited locally also by basal keratinocytes. To test which cells produce EMILIN1, we isolated epidermal HF keratinocytes and dermal fibroblasts from newborn mouse skin. Only fibroblasts expressed EMILIN1, as determined by RT-PCR analysis (Fig. 1 D). Altogether, these findings suggest that the EMILIN1 network and the fibrillar projections reaching the basal keratinocytes might play a functional role that deserves further investigation.

Emilin1$^{-/-}$ mice exhibit epidermal and dermal hyperproliferation

A comparative analysis between wild-type (WT) and *Emilin1*$^{-/-}$ skin specimens was performed. Histological analysis of skin taken from newborn *Emilin1*$^{-/-}$ mice showed an increased epidermal and dermal thickness already at postnatal day 5 (P5) compared with WT mice (Fig. 2, A and B). During the late anagen (P10), HFs were fully developed in both WT and *Emilin1*$^{-/-}$ mice, although the cellularity was higher in *Emilin1*$^{-/-}$ mice (Fig. 2 B). At P17 (catagen) and at the telogen stage P20, the thickness of the dermis and epidermis was even more pronounced in *Emilin1*$^{-/-}$ mice. No delay in hair cycle phases was evident between the two mouse genotypes, as shown in longitudinally cut representative skin cryostat sections (Fig. 2 A). At the second telogen (7 wk old), the increased epidermis and dermis thickness observed in *Emilin1*$^{-/-}$ mice was significantly different from WT mice (Fig. 2, D and E).

Although no differences were observed in the number of active caspase-3–positive cells detected in the skin of WT and *Emilin1*$^{-/-}$ mice (not depicted), the thickness of mutant mice was associated with a marked increase in Ki67 immunoreactive nuclei (Fig. 3, A and B). *Emilin1*$^{-/-}$ epidermis as well as dermis displayed a significant increase in the proliferation rate compared with WT (Fig. 3, C and D). The higher magnification images (Fig. 3, A′ and B′) and the yz sections (Fig. 3, A_y and B_y) further indicated that Ki67-positive cells were not only limited to the basal layer but extended to also involve the suprabasal layers in *Emilin1*$^{-/-}$ mice. Accordingly, the proliferation-associated Keratin K6 was present both basally as well as suprabasally in *Emilin1*$^{-/-}$ mice (Fig. 3 E). A higher proliferation rate was already evident in *Emilin1*$^{-/-}$ skin at embryonic day 16.5 (E16.5; Fig. S1).

The epidermis consists of nonproliferating multiple layers of differentiating suprabasal cells and of a proliferative basal cell layer. The higher proliferation detected in *Emilin1*$^{-/-}$ mice could be associated with defects in keratinocyte differentiation. Adult WT mice expressed K5 only in the basal cell layer, and K1 stained only the suprabasal differentiating layers (Fig. 3 E). On the contrary, whereas *Emilin1*$^{-/-}$ basal keratinocytes were positive only for K5, we detected positivity for both K5 and K1 in several suprabasal keratinocytes (Fig. 3 E). Nevertheless, a marker of terminal keratinocyte differentiation such as loricrin stained similarly in both genotypes only in the most superficial layers (Fig. 3 E). BM markers laminin-5, nidogen, and collagen IV nicely decorated epithelial BMs with an equivalent pattern in WT and *Emilin1*$^{-/-}$ mice (Fig. S2 A). To further investigate whether the altered cell proliferation could result in polarity and junctional defects, β-catenin, occludin, and ZO-1 were analyzed and found to be normally expressed in mutant mice (Fig. S2 B). In addition, β4 integrin was normally expressed in WT and *Emilin1*$^{-/-}$ K5-positive keratinocytes leaning on the BM (Fig. S2 C). Accordingly, no defects in the epidermal integrity were detected by a barrier function assay performed on 4-d-old (Fig. S2 D) and 2-wk-old mice (not depicted). Altogether, the aberrant proliferation of epidermal keratinocytes as well as of dermal fibroblasts resulting in skin hyperplasia in *Emilin1*$^{-/-}$ mice suggested that EMILIN1 negatively regulated cell growth.

EMILIN1 directly inhibits fibroblast and keratinocyte proliferation in vitro

The expression of EMILIN1 in the dermal stroma and the presence of EMILIN1-positive fibrillar projections up to the basal layers of epidermis and in the hair bulb suggest that EMILIN1 might directly regulate the proliferation of dermal

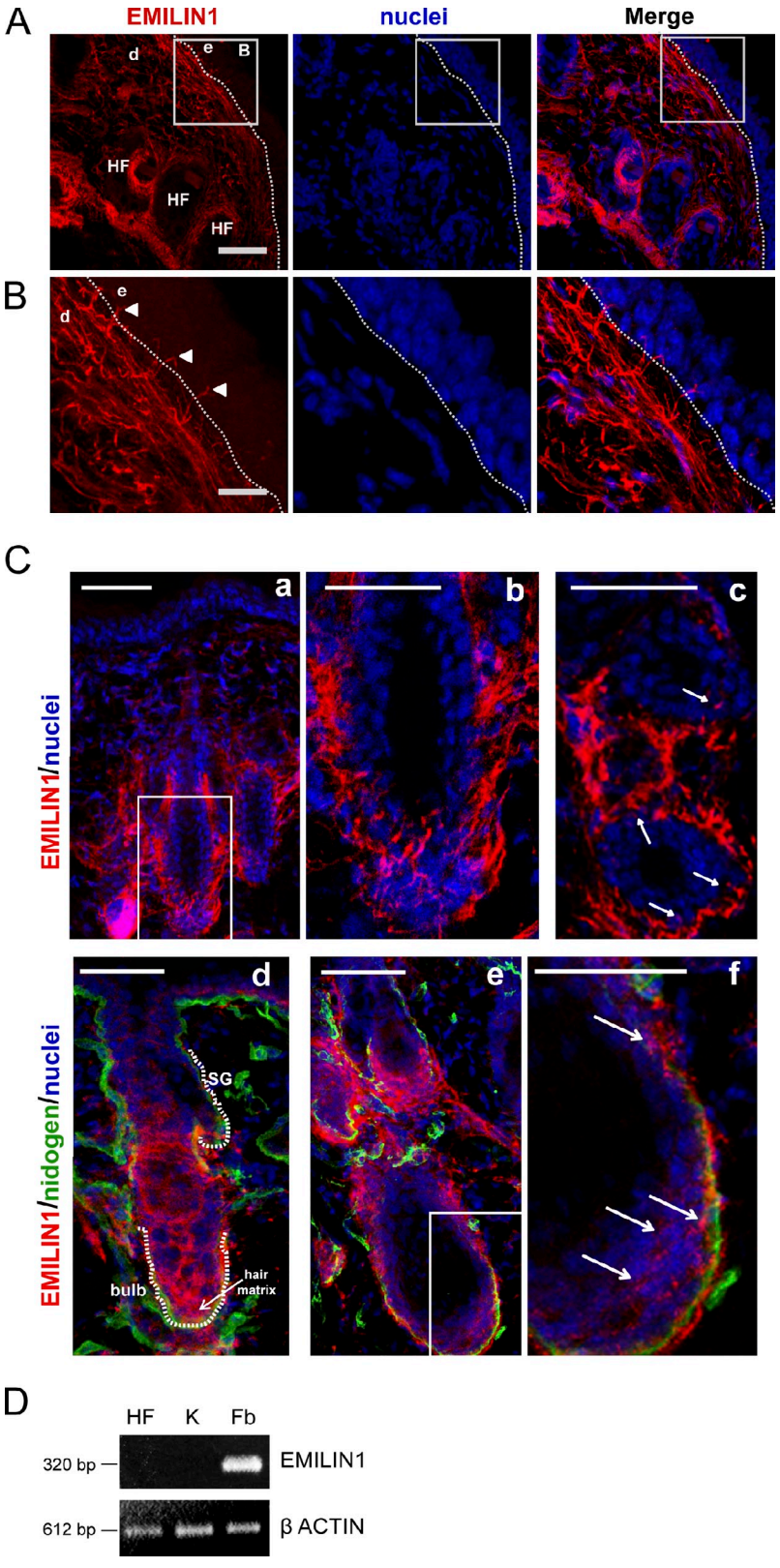

Figure 1. **EMILIN1 is expressed by dermal fibroblasts and takes contact with basal keratinocytes.** (A) Representative immunofluorescence images of skin cryostat sections of 7-wk-old WT mice stained for EMILIN1 and nuclei. Bar, 50 µm. (B) Zoomed images of boxes in A Arrowheads evidence EMILIN1-positive fibrillar projections that take contact with basal keratinocytes. Bar, 16 µm. (A and B) d, dermis; e, epidermis. The dashed lines denote the BM. (C) Images representing HFs surrounded by EMILIN1. (b) A zoomed image corresponding to the boxed area in a; (c) A transversally cut section where EMILIN1-positive protrusions reach keratinocytes (indicated by arrows); (d, e, and f) Sections cut longitudinally stained for nidogen; (f) A zoomed image corresponding to the boxed area in e, with arrows indicating the EMILIN1-positive protrusions. The white dotted lines in d indicate the sebaceous gland (SG) and bulb. Bars: (a, c, d, and e) 50 µm; (b) 40 µm; (f) 30 µm. (D) Comparative RT-PCR analysis of EMILIN1 mRNA levels in HFs, keratinocytes (K), and fibroblasts (Fb) isolated from newborn WT mouse skin.

cells as well as keratinocytes. To assess this hypothesis, we isolated keratinocytes and dermal fibroblasts from newborn WT and *Emilin1*$^{-/-}$ mice and performed in vitro proliferation assays. Dermal fibroblasts isolated from *Emilin1*$^{-/-}$ mice retained a higher proliferation (40% BrdU-positive cells) compared with WT fibroblasts (22% BrdU-positive cells) also when cultured in vitro (Fig. 4 A) for 3 d. Subsequently, a coculture assay with keratinocytes and dermal fibroblasts isolated from WT and *Emilin1*$^{-/-}$ mice was performed. In detail, the two cell types were cocultured in the same well

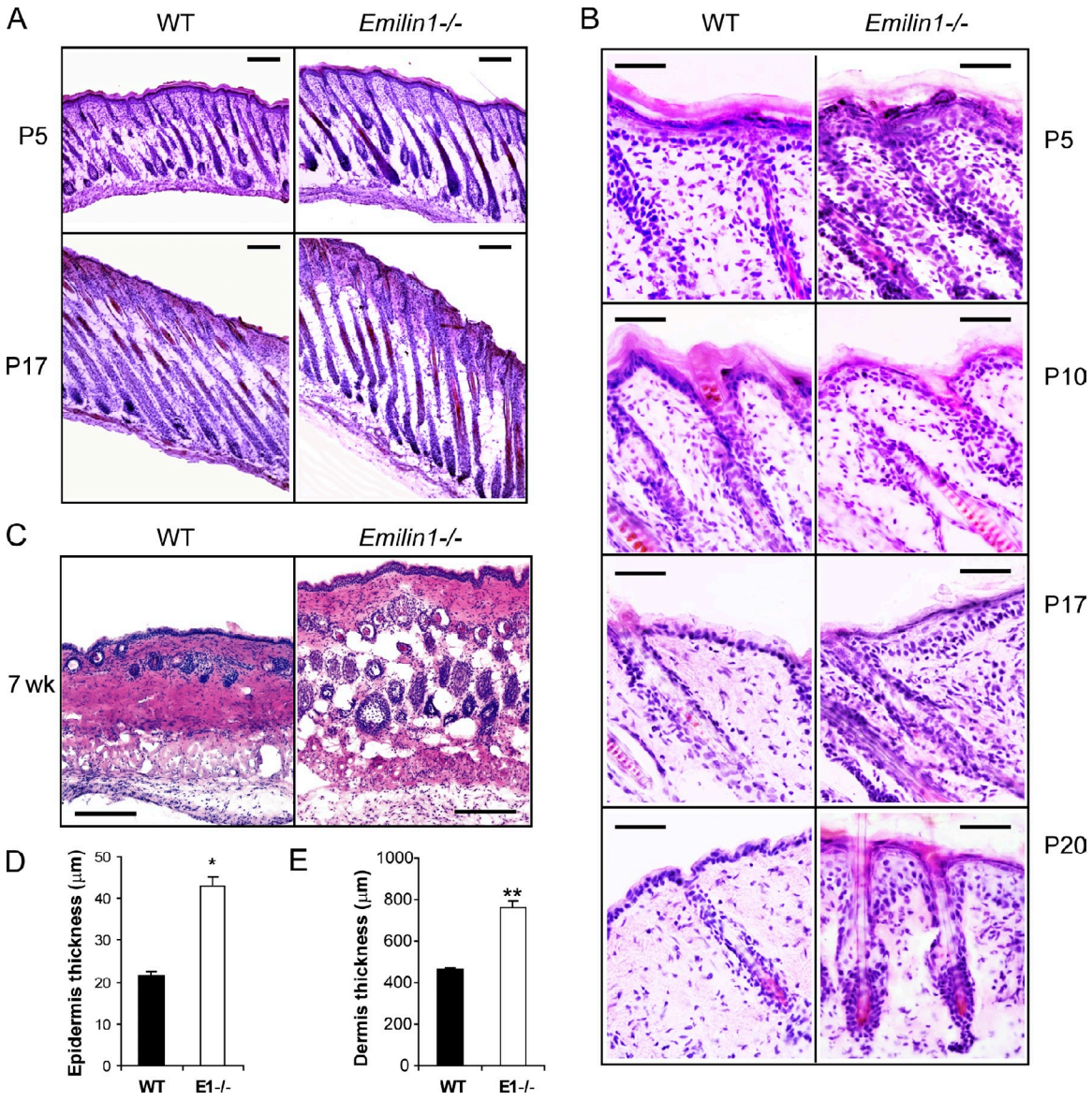

Figure 2. **Skin hyperplastic phenotype in *Emilin1*$^{-/-}$ mice.** (A and B) H/E-stained skin cryostat sections cut longitudinally at different phases of the hair cycle. (A) Low magnification of first anagen (P5) and first catagen (P17). Bars, 200 µm. (B) High magnification of first anagen, late anagen (P10), first catagen, and first telogen (P20). Bars, 50 µm. (C) Cross sections of 7-wk-old skin. Bars, 100 µm. (D and E) ImageJ quantification of epidermis and dermis thickness of 7-wk-old WT ($n = 5$) and *Emilin1*$^{-/-}$ ($n = 5$) mice. For this analysis, three H/E-stained sections for each mouse were examined. Mean values ± SD are reported. *, $P = 1 \times 10^{-14}$; **, $P = 2 \times 10^{-12}$.

(a condition named contact) or were physically separated by an insert (transwell) to assess whether fibroblasts were able to influence the proliferation of keratinocytes. Proliferation was reduced to a much larger extent in contact cocultures with WT fibroblasts (40%) compared with *Emilin1*$^{-/-}$ fibroblasts (70%; Fig. 4 B). On the contrary, either WT or *Emilin1*$^{-/-}$ fibroblasts slightly, but not significantly, reduced keratinocyte proliferation when cocultured and separated in a transwell system (Fig. 4 C). As expected, no differences were observed between WT (Fig. 4, B and C, black bars) and *Emilin1*$^{-/-}$ keratinocytes (Fig. 4, B and C, gray bars). Although these latter findings suggested that soluble factors released by fibroblasts might partially influence keratinocyte proliferation, by far, the major inhibitory effects were likely related to EMILIN1 expression in WT cells versus nonexpression in *Emilin1*$^{-/-}$ cells.

To assess the hypothesis that EMILIN1 might directly regulate the proliferative potential of keratinocytes, we suppressed EMILIN1 expression in a mouse fibroblast cell line (National Institutes of Health [NIH] 3T3) by specific short hairpin RNA (shRNA) sequences. Then, mouse keratinocytes were contact cocultured with control NIH 3T3 cells transfected with scrambled shEmilin1 sequence or with either one of the two clones displaying an almost complete protein silencing (clones 6505 and 6502; Fig. 4 D, top). After 3 d of contact growth, proliferation was revealed by BrdU incorporation, and keratinocytes were detected by anti–pan-cytokeratin (CK) immunostaining. Representative confocal images documented that proliferating BrdU and CK double positive keratinocytes were present in higher number when they were cocultured with NIH 3T3 cells transfected with shEmilin1 (i.e., clones 6505 and 6502; Fig. 4,

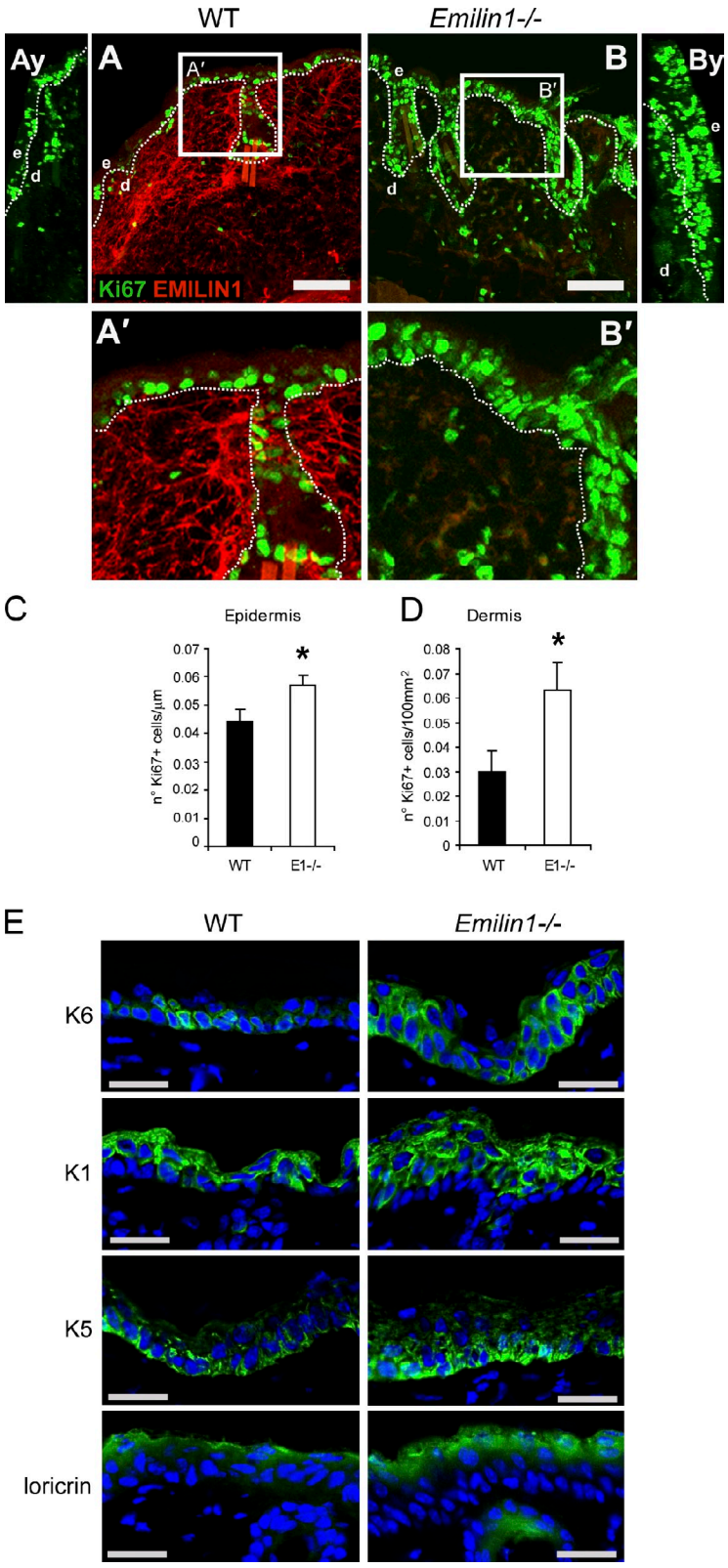

Figure 3. ***Emilin1*$^{-/-}$ mice display epidermal and dermal hyperproliferation.** (A and B) Representative images of WT and *Emilin1*$^{-/-}$ mouse skin cryostat sections stained for EMILIN1 and for the proliferation marker Ki67. Bars, 75 µm. (A_y and B_y) yz sections of the confocal images shown in A and B. (A′ and B′) Zoomed images of the boxed areas in A and B. d, dermis; e, epidermis. The dashed lines denote the BM. (C and D) ImageJ analysis of the number of epidermal Ki67-positive cells/micrometer and dermal Ki67-positive cells/100 µm^2. Mean values ± SD are reported. *, $P < 0.02$. For these quantitative analyses, three different cryostat sections of 7-wk-old WT ($n = 5$) and *Emilin1*$^{-/-}$ ($n = 5$) mice were examined. (E) Representative images of WT and *Emilin1*$^{-/-}$ mouse skin cryostat sections. Green staining represents Keratin 1 (K1), Keratin 5 (K5), Keratin 6 (K6), and loricrin. Nuclei are shown in blue. Bars, 25 µm.

D [bottom] and E). Then, to determine whether the proliferative effect was directly linked to EMILIN1, freshly obtained mouse keratinocytes were grown on the gC1q cell–binding domain of EMILIN1 or on fibronectin. After 3 d, we detected a significantly lower number of BrdU-positive cells grown on gC1q compared with those on fibronectin (Fig. 4, F and G).

EMILIN1 inhibits cell proliferation through a cognate interaction with α4β1 and α9β1 integrins

Altogether, the aforementioned results support the hypothesis that EMILIN1 might exert a negative control on cell growth by a direct interaction with specific integrins on the cell surface.

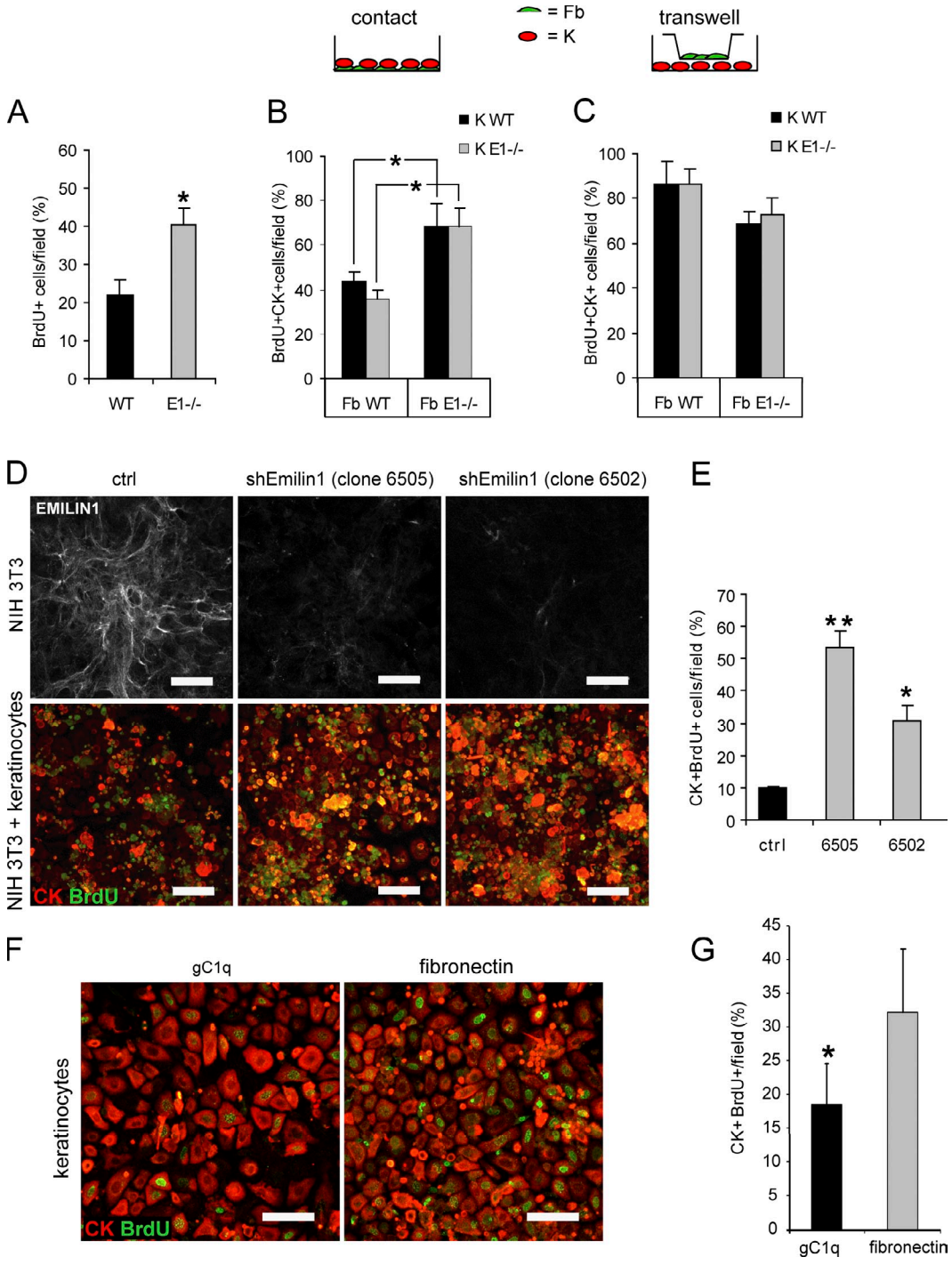

Figure 4. **EMILIN1 directly affects proliferation of mouse dermal fibroblasts and keratinocytes.** (A) In vitro proliferation of mouse dermal fibroblasts. Different populations of WT ($n = 4$) and of *Emilin1*$^{-/-}$ ($n = 6$) fibroblasts at passage 3 were analyzed. The percentage of mean values (±SD) of the number of BrdU-positive cells/field is reported. *, P = 0.01. (B and C) Cocultures of keratinocytes (K) and dermal fibroblasts (Fb) isolated from WT and *Emilin1*$^{-/-}$ newborn mice. The two cell types (Fb and K) were cultured in the same well (contact) or in a transwell system for 3 d. The quantification of keratinocyte proliferation was performed counting the BrdU and CK double positive cells/field. Here, the percentage of mean values (±SD) of three independent experiments is reported. *, P = 0.03. (D, top) EMILIN1 immunofluorescence staining of mouse fibroblasts transfected with an shRNA Emilin1 (shEmilin1) scrambled sequence (control [ctrl]) and two clones (6505 and 6502) transfected with specific sequences for Emilin1 silencing. (bottom) Contact cocultures of mouse keratinocytes and NIH 3T3 fibroblasts (control and EMILIN1-silenced cells). BrdU-positive cells are stained green; the pan-CK–positive keratinocytes are shown in red. (E) Quantification of BrdU-positive keratinocytes per field. The percentage of mean values (±SD) of three independent experiments is reported. *, P = 0.01; **, P < 0.001. (F) Mouse keratinocytes grown for 48 h on gC1q or fibronectin-coated plates for BrdU and CK. (G) Quantification of BrdU-positive keratinocytes per field. The percentage of mean values (±SD) of three independent experiments is reported. *, P = 0.01. Bars, 50 µm.

First, we assessed the proliferation of carcinoma (HeLa and CaCo-2), sarcoma (HT1080 and rhabdomyosarcoma [RD]), and keratinocyte HaCaT cell lines in the presence or in the absence of soluble gC1q added to the culture medium. Even if the proliferation rate was variable among the cell lines analyzed, the addition of soluble gC1q reduced the number of BrdU-positive cells in respect to their own control from 20 to 60%, with HT1080 and HaCaT as the most sensitive cells (Fig. 5 A). HT1080, CaCo-2, and HaCaT cells were selected for further experiments as representative of fibroblasts and epithelial cells. FACS analysis determined that HT1080 and HaCaT expressed α4β1, the known EMILIN1 integrin receptor, whereas CaCo-2 expressed negligible levels of α4β1 (Fig. 5 B). α9β1 integrin was included in our analysis because it is highly homologous to α4 (Palmer et al., 1993), and it is expressed by basal keratinocytes, whereas α4 is lacking in these cells (Fuchs, 2007). One notable exception was HaCaT immortalized cells that, although derived from basal keratinocytes, expressed only α4β1. HT1080 did not express α9β1, whereas CaCo-2 cells were moderately positive (Fig. 5 B). RD and HeLa cells expressed both integrins but at lower levels than HT1080 or CaCo-2 cells (Fig. 5 B). We preliminarily demonstrated that HT1080 and CaCo-2 cells specifically adhered to gC1q with their respective integrins (i.e., α4β1 for HT1080 and α9β1 for CaCo-2; Fig. 5 C). The addition of an anti–α4 integrin function-blocking antibody (P1H4) to HT1080 or an anti–α9 integrin function-blocking antibody (Y9A2) to CaCo-2 specifically inhibited cell adhesion. An antibody against β1 integrin (4B4) blocked adhesion of both cell lines (Fig. 5 C). Furthermore, we specifically abrogated cell adhesion when mutants in which the integrin-binding region was deleted or mutated in the 933 glutamic acid residue were used. This inhibitory effect was absent with gC1q mutated in other residues in the binding region (Figs. 5 C and S3; Verdone et al., 2008).

To probe the mechanistic link between integrin α4β1 or α9β1 and inhibition of cell proliferation, we determined the lower dose of soluble gC1q that could significantly inhibit cell proliferation (5 µg/ml; unpublished data). Then, the addition of function-blocking P1H4 to HT1080 and HaCaT or Y9A2 to CaCo-2 or an antibody able to prevent integrin recognition of gC1q (1H2; Spessotto et al., 2003) rescued the inhibition of cell proliferation induced by gC1q (Fig. 5, D–F). The rescue obtained using cell adhesion nonfunctional gC1q mutants (Fig. 5 G) also confirmed the specificity of the inhibitory effect of gC1q on cell proliferation.

Altogether, these data strongly indicated that EMILIN1 negatively controlled cell growth by the direct engagement of its C-terminal gC1q domain to α4β1 or α9β1 integrins. The expression of α9β1 integrin in keratinocytes as shown by positive staining of adult WT mouse skin sections reinforced the evidence of the antiproliferative activity of EMILIN1 by a direct interaction with this specific cellular receptor (Fig. 5 H).

The altered proliferative homeostasis in *Emilin1*$^{-/-}$ mice is associated with PI3K/Akt and Erk1/2 pathway activation

Considering that TGF-β is implicated in the maintenance of skin homeostasis (Böttinger et al., 1997; Tang et al., 1998, 1999) and that EMILIN1 binds pro–TGF-β to negatively regulate its maturation (Zacchigna et al., 2006), we determined the influence of this cytokine in the hyperproliferative skin phenotype of *Emilin1*$^{-/-}$ mice. For this purpose, we quantified Ki67-positive cells in *Emilin1*$^{+/+}$*TGF-β*$^{+/+}$, *Emilin1*$^{+/+}$*TGF-β*$^{+/-}$, *Emilin1*$^{-/-}$*TGF-β*$^{+/+}$, and *Emilin1*$^{-/-}$*TGF-β*$^{+/-}$ mouse back skin (Fig. S4, A–F). As expected, the inactivation of one TGF-β allele increased the number of Ki67-positive cells in WT epidermis and dermis (Fig. S4, B, E, and F). On the other hand, the levels of Ki67-positive cells were comparable in *Emilin1*$^{-/-}$*TGF-β*$^{+/+}$ and *Emilin1*$^{-/-}$*TGF-β*$^{+/-}$ mice, indicating that TGF-β gene dosage was apparently less relevant for skin proliferation in an EMILIN1-negative background (Fig. S4, D, E, and F). Alternatively, a functional upper limit in cell proliferation levels could have already been reached. Analysis of whisker follicles confirmed these results (Fig. S4 G). We did not notice any additional inhibitory effect on cell proliferation after treatment of dermal fibroblasts and keratinocytes with gC1q plus TGF-β (Fig. S4 H). We confirmed these findings also in several cell lines, except for a slight but not significant inhibitory effect in CaCo-2 and HaCaT cells (Fig. S4 I).

The augmented TGF-β levels in *Emilin1*$^{-/-}$ mouse skin were surprisingly accompanied by a decreased phosphorylation at the C-terminal Ser465/467 of Smad2, whereas an increased phosphorylation of its Ser245/250/255 residues corresponding to the linker region targeted by Erk1/2 (Kretzschmar et al., 1999) was observed (Fig. 6, A and B). The levels of activated Erk1/2 as well as of other proproliferative signal molecules (Akt and PI3K) and effectors (Cyclin A and Cdk 2) were higher in *Emilin1*$^{-/-}$ mice (Fig. 6, A and B). The aforementioned findings prompted us to hypothesize a mechanism by which EMILIN1 deficiency and increased TGF-β levels could influence cell growth. The enhanced levels of pErk1/2 detected when α4/α9 integrins were not bound by gC1q were likely the result of decreased PTEN phosphatase expression, as evident in *Emilin1*$^{-/-}$ skin extracts (Fig. 6, A and B). The altered pErk1/2 expression of skin extracts was still detected when epidermis and dermis were separately analyzed, with the dermis displaying the most significant changes (Fig. 6, C and D). In accord with the in vivo findings, PTEN increased in all cell types adherent to gC1q (dermal fibroblasts, keratinocytes, CaCo-2, and HaCaT; Fig. 7, A–D). The addition of TGF-β further increased PTEN levels, and this was in agreement with the reduced cell proliferation (Fig. S4, H and I). Finally, the higher expression of PTEN was accompanied by decreased pErk1/2 levels (Fig. 7, A–D). These data suggested a link between PTEN and α4/α9 integrin engagement: when α4/α9 integrins were not ligated by gC1q, as it occurs in *Emilin1*$^{-/-}$ mice, PTEN was reduced, and, hence, pErk1/2 was up-regulated. Thus, in the absence of PTEN, pErk1/2 levels should not be affected. To formally prove this hypothesis, PTEN was silenced in CaCo-2 (α9 integrin positive) and HaCaT (α4 integrin positive) cells. Starved cells (silenced [pLKO#49] or not silenced [pLKO]) were allowed to adhere onto gC1q in the presence or absence of TGF-β. Both pLKO and pLKO#49 cells adhered onto gC1q at the same extent as compared with WT CaCo-2 and HaCaT cells (unpublished data). When PTEN was silenced by specific shRNA, the levels of pErk1/2 remained higher than in control cells (Fig. 7, E and F). This effect was

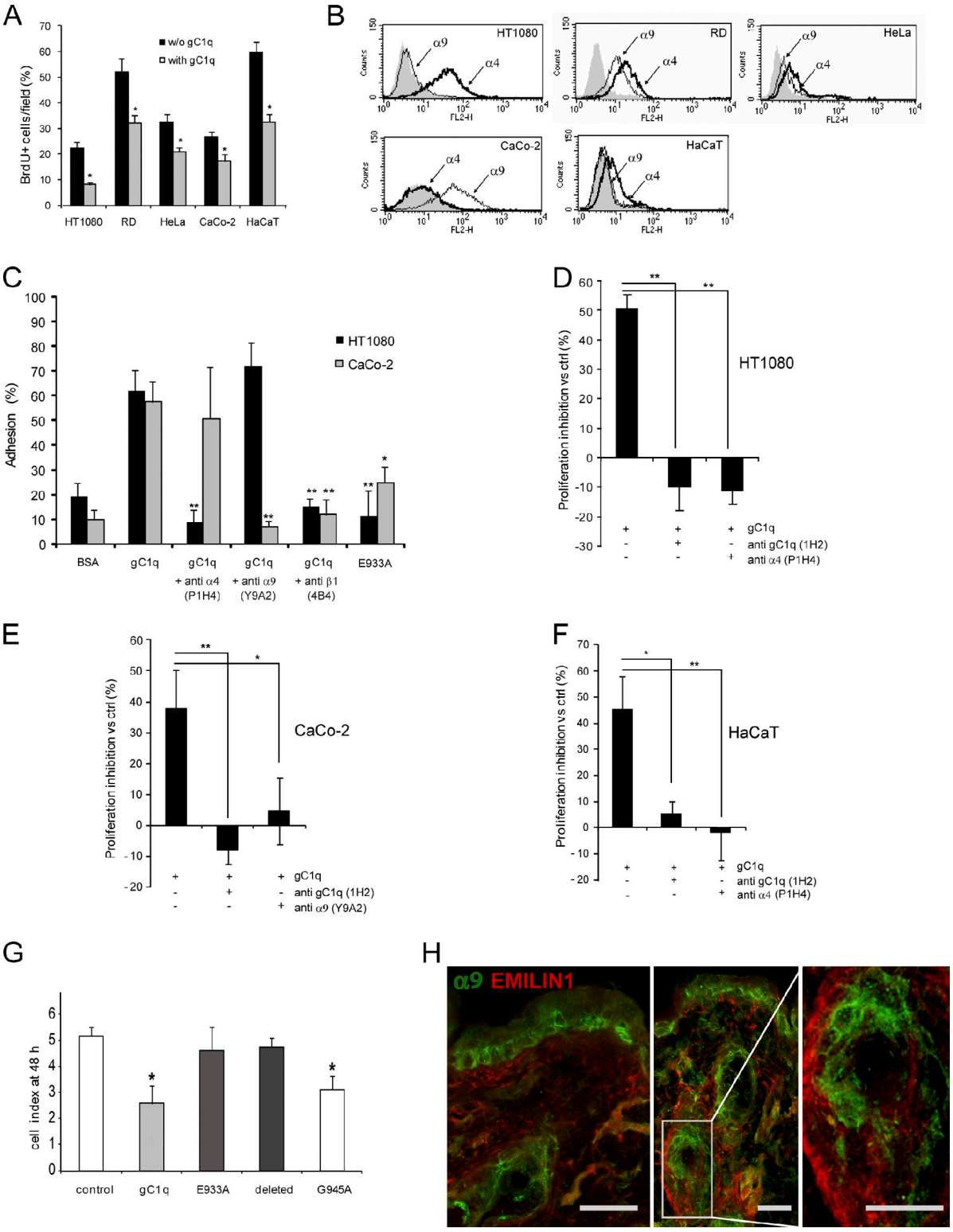

Figure 5. **The EMILIN1 gC1q domain inhibits cell proliferation through the interaction with the α4 and α9 integrin subunit.** (A) Proliferation of sarcoma (HT1080 and RD), carcinoma (HeLa and CaCo-2), and immortal keratinocyte (HaCaT) cell lines in the presence or in the absence of 50 µg/ml of soluble gC1q added to the culture medium for 24 h. The percentage of mean values (±SD) of the number of BrdU-positive cells per field of three independent experiments is reported. *, $P < 0.05$. (B) FACS analysis of α4 and α9 integrin subunit expression levels in HT1080, RD, CaCo-2, HeLa, and HaCaT cells. (C) Cell adhesion of HT1080 and CaCo-2 cells to gC1q. The cells were preincubated with anti–α4 integrin subunit mAb (P1H4), anti–α9 integrin subunit mAb (Y9A2), or anti–β integrin subunit mAb (4B4; final concentration, 10 µg/ml) for 15 min at 37°C and were then allowed to adhere at 37°C for 20 min. Data are expressed as the means ± SD of three independent experiments with six replicates. *, $P < 0.05$; **, $P < 0.001$. (D–F) Proliferation inhibition of HT1080, CaCo-2, and HaCaT cells expressed as the percentage versus the respective control (ctrl). The gC1q domain was used at a concentration of 5 µg/ml; the monoclonal antibody anti-gC1q (1H2) and the function blocking monoclonal antibodies anti–α4 integrin subunit (P1H4) and anti–α9 integrin subunit (Y9A2) were used at 10 µg/ml. Data are expressed as the means ± SD of three independent experiments. *, $P < 0.05$; **, $P < 0.001$. (G) Effect of

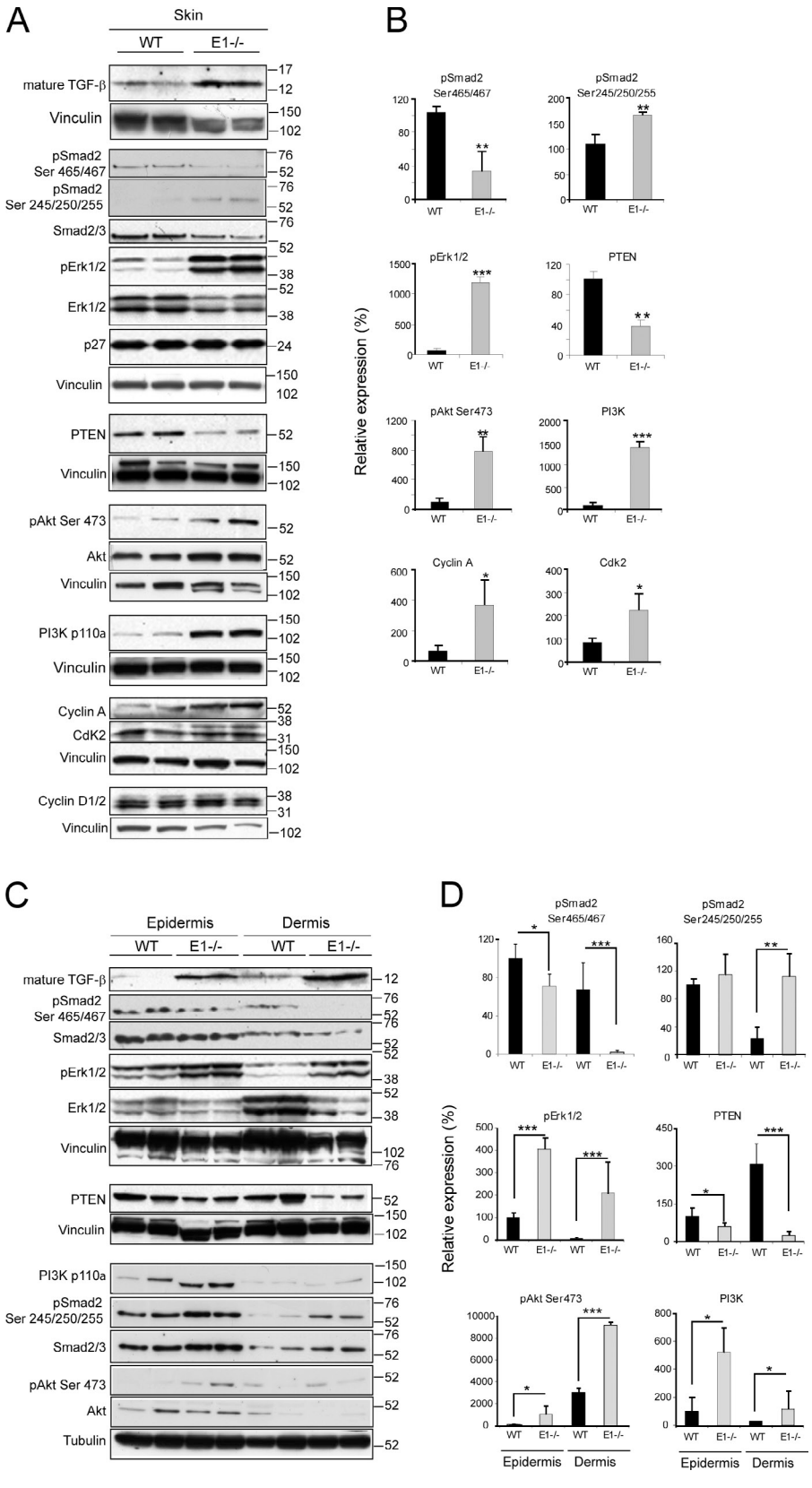

Figure 6. **Lack of EMILIN1 up-regulates PI3K/Akt and Erk1/2 and down-regulates PTEN.** (A) Representative Western blot analysis of 6–8-wk-old skin tissue extracts of WT and *Emilin1*$^{-/-}$ mice. (B) Quantification of Western blot analysis reported in A by Quantity One software. The mean values (±SEM) of pSmad2 (Ser465/467 and Ser245/250/255), pErk1/2, PTEN, pAkt (Ser473), PI3K, Cyclin A, and Cdk2 relative expression levels of WT (n = 8) and *Emilin1*$^{-/-}$ (n = 8) mice are reported. (C) Representative Western blot analysis of epidermis and dermis extracts of 7-wk-old WT and *Emilin1*$^{-/-}$ mice. (A and C) Molecular mass is indicated in kilodaltons. (D) Quantification of Western blot analysis reported in C by Quantity One software. The mean values (±SD) of pSmad2 (Ser465/467 and Ser245/250/255), pErk1/2, PTEN, pAkt (Ser473), and PI3K relative expression levels of WT (n = 4) and *Emilin1*$^{-/-}$ (n = 4) mice are reported. *, P = 0.05; **, P < 0.05; ***, P < 0.01.

gC1q and the mutants E933A, G945A, and the deleted form on CaCo-2 cell proliferation monitored using the XCELLigence system. The cell index after 48 h of dynamic monitoring calculated as the mean ± SD from n = 3 experiments with n = 6 replicates is reported. *, P < 0.001. (H) Representative immunofluorescence images of skin cryostat sections of 7-wk-old WT mice stained for EMILIN1 and for the α9 integrin subunit. Bars, 25 µm.

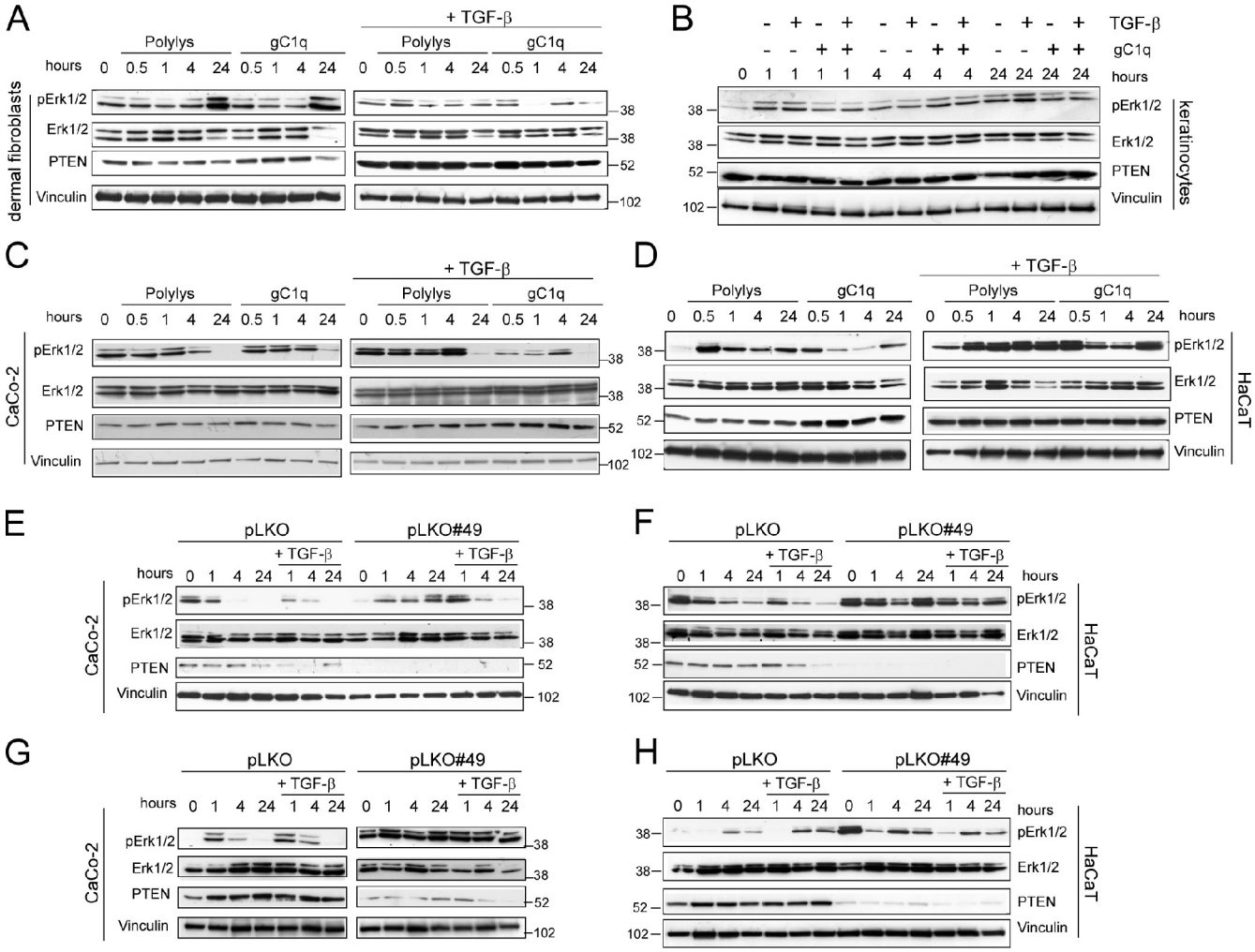

Figure 7. **PTEN down-regulates pErk1/2.** (A and B) Western blot analysis of dermal fibroblast and keratinocyte extracts after adhesion on control polylysine (Polylys) or on gC1q in the presence or absence of 10 ng/ml TGF-β. (C and D) Western blot analysis of CaCo-2 and HaCaT cell extracts after adhesion on control polylysine or on gC1q in the presence or absence of 10 ng/ml TGF-β. (E and F) Western blot analysis of control (pLKO) or PTEN-silenced (pLKO#49) CaCo-2 and HaCaT cell extracts after adhesion for different lengths of time on gC1q in the presence or absence of 10 ng/ml TGF-β. (G and H) Western blot analysis of control (pLKO) or PTEN-silenced (pLKO#49) CaCo-2 and HaCaT cell extracts after the addition of 5 µg/ml soluble gC1q in the presence or absence of 10 ng/ml TGF-β.

observed also when attached CaCo-2 and HaCaT cells, growing on plastic under normal culture conditions, were treated with soluble gC1q; pErk1/2 levels were up-regulated in control cells (pLKO) but not in PTEN-silenced cells (pLKO#49; Fig. 7, G and H). Thus, gC1q integrin ligation determined the EMILIN1-dependent antiproliferative effects that in turn regulated PTEN expression and hence pErk1/2 levels.

Accelerated closure of skin wounds in *Emilin1*$^{-/-}$ mice

To functionally link a potential contribution of EMILIN1 expression to the control of skin wound and to the process of tissue regeneration, we performed full-thickness excisional wounds on the back of 7-wk-old WT (n = 6) and *Emilin1*$^{-/-}$ (n = 6) mice. At different postwounding days, photographs were taken (Fig. 8 A), and the size of the wound edge was measured. As evident in Fig. 8 (A and B), the skin wounds of *Emilin1*$^{-/-}$ mice closed considerably faster than their WT littermates, and the differences were significant already at the early phase. To correlate the accelerated wound closure to the hyperproliferative phenotype of *Emilin1*$^{-/-}$ mice, we stained cryostat sections of wounded skin for Ki67 (Fig. 8 C). The proliferation was significantly increased in *Emilin1*$^{-/-}$ compared with WT mice (Fig. 8 D), indicating that EMILIN1 is involved also in reepithelialization and regenerative processes.

Discussion

Skin homeostasis is regulated by microenvironmental growth factors, ECM proteins, and integrins (Fuchs, 2007). The most prominent phenotype of the *Emilin1*$^{-/-}$ mouse skin reported here was the increased thickness of the epidermis and dermis. It is generally known that integrin engagement positively regulates cell growth (Schwartz et al., 1995). The finding that the ECM glycoprotein EMILIN1 modulated skin cell proliferation pointed out an opposite function of α4β1 and α9β1 integrins: the lack of integrin occupancy by EMILIN1 resulted in reduced PTEN, up-regulated Erk1/2, and increased

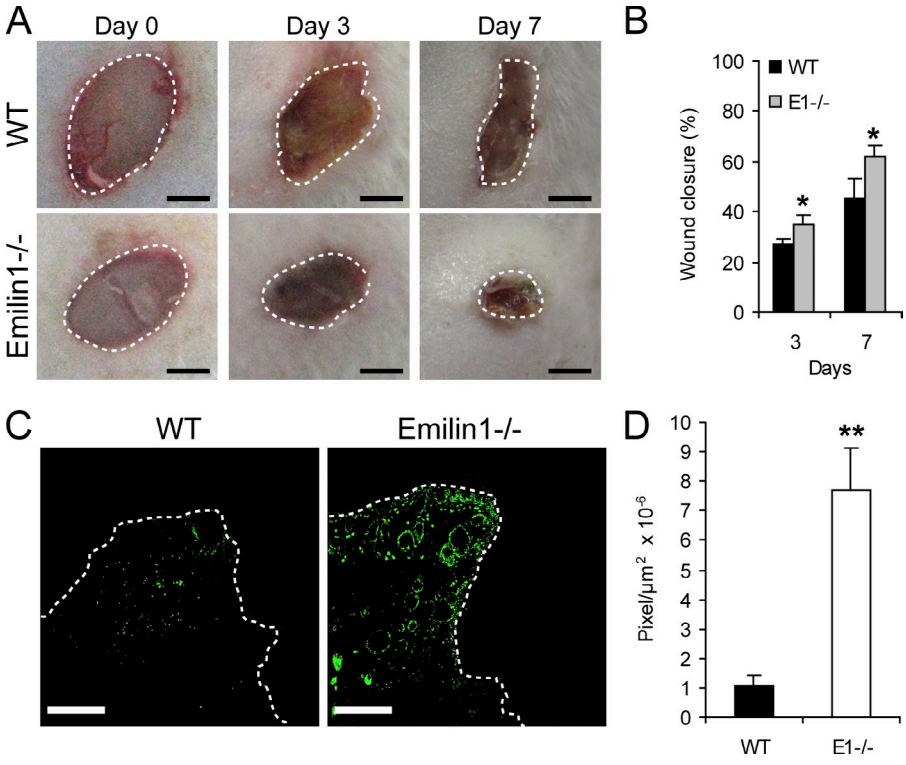

Figure 8. **Wound closure is accelerated in *Emilin1*$^{-/-}$ mice.** (A) Representative examples at 0, 3, and 7 d after skin wounding. Bars, 2 mm. (B) Quantification of wound closure at 3 and 7 d. The mean values ± SEM are reported. *n* = 6. *, P = 0.04. (C) Immunofluorescence staining of skin cryostat sections at day 3 with Ki67. Bars, 300 µm. (A and C) The dashed lines indicate the wound edges. (D) Quantification of proliferation in the wounded area. The mean values ± SEM correspond to ImageJ software evaluation of Ki67 fluorescence staining in the wounded area (pixel/area). *n* = 6. **, P = 0.002.

fibroblasts and keratinocytes proliferation, whereas when these integrins were bound to EMILIN1, a normal cell growth was maintained. Finally, this study identified EMILIN1 as a novel α9β1 integrin ligand.

Epidermal–dermal communication through the BM is important for skin homeostasis (Grose et al., 2007). The BM contains a specialized structure, the anchoring complex, which ensures the stability of connection and communication between these two tissue compartments (Böck, 1983; Nishiyama et al., 2000). The proteins within the anchoring complex provide links to both the intracellular cytoskeletal keratins in keratinocytes and connective tissue proteins of the dermis (i.e., collagen fibers and elastic microfibrils; Masunaga et al., 1997). One of the key components of the anchoring filaments is laminin-5, which initiates hemidesmosome formation and provides stable attachment of the epidermis to the dermis (Nishiyama et al., 2000). Other components of the BM at the dermal–epidermal junction are mainly type IV and VII collagens, several laminins such as laminin-6 and -10, nidogen, and perlecan (Marinkovich et al., 1993; Kikkawa et al., 1998, 2000). In the present study, we demonstrated an abundant expression of EMILIN1 in the dermal stroma. Interestingly, EMILIN1-positive fibrils departed from the region below the BM reaching the basal keratinocyte layer. EMILIN1 also surrounded the outer root sheath of the HFs and displayed protrusions toward the keratinocytes in the follicle bulb. The peculiar localization of EMILIN1 up to the basal layer of keratinocytes indicated that this ECM protein plays a role in connecting the epidermis to the underlying dermal layer. In addition to a potential structural function, we demonstrated that EMILIN1 regulated keratinocyte as well as fibroblast proliferation through a direct integrin-mediated cell–ECM interaction.

This notion is supported by several experimental evidences. First, EMILIN1 produced by fibroblasts was deposited in the dermis and contacted basal keratinocytes. Second, only contact and not transwell coculture of keratinocytes with WT EMILIN1-producing fibroblasts inhibited their proliferation. Third, knocking down EMILIN1 expression in NIH 3T3 fibroblasts stimulated the proliferation of cocultured keratinocytes. Fourth, keratinocytes plated on the cell-binding gC1q domain proliferated significantly less than keratinocytes grown on fibronectin. Fifth, functional antibodies blocking EMILIN1 ligation by α4β1 or α9β1 integrin prevented the inhibition of cell proliferation.

TGF-β is one of the major cytokines regulating the maintenance of skin homeostasis (Böttinger et al., 1997; Tang et al., 1998, 1999). TGF-β is synthesized as a large precursor (pro–TGF-β) that is cleaved by proprotein convertases (Beck et al., 2002; Annes et al., 2003). Mounting evidence indicates that the diversity of TGF-β signaling responses is determined by the combinatorial usage of core pathway components and by cross talk with other signaling pathways to modulate (i.e., reinforcing or attenuating downstream cellular responses; Zhang, 2009). Here, we demonstrated that *Emilin1*$^{-/-}$ dermal fibroblasts as well as keratinocytes proliferated to a higher extent than WT cells, even if higher TGF-β levels were present. Our expectation was that the lower TGF-β levels attained in *Emilin1*$^{-/-}$ *TGF-β*$^{+/-}$ mice could effectively rescue the normal skin phenotype. However, this was not the case and suggested that a cross talk between α4/α9 integrins and TGF-β occurred. Physiological signals such as those activated by EGF or integrins are able to trigger phosphorylation of the inhibitory sites in the linker region of Smad2 and may use this mechanism to adjust the ability of Smad2 to convey appropriate TGF-β signals.

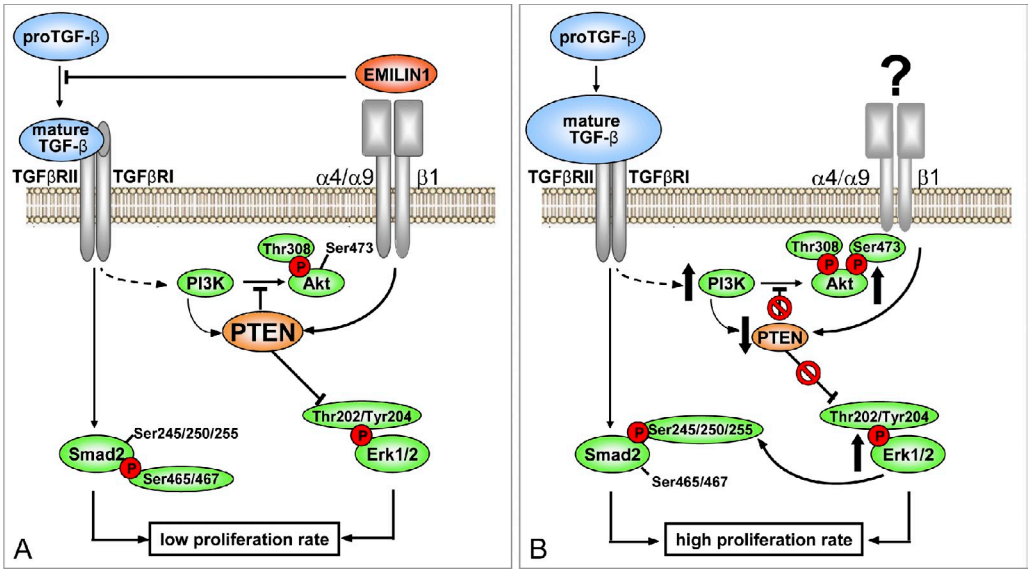

Figure 9. **Proposed model for the regulatory role of EMILIN1 in skin homeostasis.** The illustration summarizes the proposed molecular mechanism underlying the regulatory role of EMILIN1 in skin proliferation. (A) TGF-β triggers cytostatic signal pathways mainly through pSmad2 (Ser465/467) activation and modulates PI3K/Akt signaling by regulating PTEN expression. Zacchigna et al. (2006) showed that EMILIN1 inhibits TGF-β processing by binding specifically to the pro–TGF-β precursor and by preventing its maturation in the extracellular space. Here, we demonstrated that EMILIN1 binding to dermal fibroblast and basal keratinocytes α4β1/α9β1 integrins empowers the down-regulation of proliferative cues induced by TGF-β. This effect is mediated by α4/α9β1-dependent PTEN activation and inhibition of pErk1/2 proproliferative activity. (B) The increased levels of mature TGF-β and the lack of α4/α9β1 integrin–specific engagement by the lack of EMILIN1 result in PTEN down-regulation and, hence, reduced activity. This determines the activation of proliferative pathways such as pAkt and pErk1/2 that in turn lead to a reduction of TGF-β signaling via increased Erk1/2-dependent phosphorylation of Smad2 at inhibitory Ser245/250/255. In conclusion, we provide the first evidence for the central role of PTEN in the cross talk between α4/α9β1 integrin and TGF-β signal pathways.

Hepatoma cancer cells overexpressing β1A integrin display loss of the Smad2/3 C-terminal phosphorylation sites (Hamajima et al., 2009). This depends on the phosphorylation of the linker region mediated by Erk activation and results in the repression of the antiproliferative effect of TGF-β (Kretzschmar et al., 1999). One of the most relevant molecular features observed in *Emilin1*$^{-/-}$ skin extracts was the dramatic increase of pErk1/2. The higher levels of activated Erk in *Emilin1*$^{-/-}$ tissues were linked to a reduced expression of PTEN. Our data are in line with the results obtained by White et al. (2003), who demonstrated that ligation of α4β1 integrin induced a significant increase in PTEN activity. Here, we detected strong Erk1/2 activation, phosphorylation of the linker region, and down-regulation of the C-terminal pSmad2 sites when α4β1 and α9β1 integrins were not ligated by EMILIN1. It is likely that the down-regulation of pSmad2 signaling, even when the TGF-β levels are higher as in *Emilin1*$^{-/-}$ mice, is the consequence of a direct Erk1/2 action whose activation is in turn linked to PTEN reduced levels.

It is worth considering that the higher TGF-β levels in *Emilin1*$^{-/-}$ mice could enhance cell proliferation in a Smad-independent manner. PTEN expression is regulated by TGF-β in keratinocytes (Li and Sun, 1997), and PTEN mRNA levels are reduced in a model of TGF-β–overexpressing transgenic mice (Ebert et al., 2002). Chow et al. (2008) demonstrated that TGF-β enhanced cell proliferation by increasing PI3K tyrosine phosphorylation and suppressing PTEN. Accordingly, the decreased PTEN and higher PI3K activity observed in our models may give keratinocytes and fibroblasts a growth advantage. Depletion of PTEN by shRNA in α4/α9-positive cell lines provided the formal demonstration that engagement of integrins by EMILIN1 regulated pErk1/2 levels through PTEN. When integrins engaged EMILIN1, the pErk1/2-dependent phosphorylation of the inhibitory Smad2 Ser245/250/255 residues was reduced, and proliferation was maintained at lower levels.

Emilin1$^{-/-}$ mice also were useful to address the role of EMILIN1 in dermal wound healing. Our present data showed that the absence of EMILIN1 accelerated the early events of wound closure. The enhanced proliferation rate detected in *Emilin1*$^{-/-}$ normal skin was thus transposed to the dermal wound healing process, in which a much higher proliferation was evident in *Emilin1*$^{-/-}$ mice. On the other hand, conditional null mice for the α9 integrin chain in the skin and cornea (K14-α9 null) showed a significantly reduced proliferation in cutaneous wounds with thinner epithelium (Singh et al., 2009). α9β1 interacts with tenascin-C and the EIIIA segment of fibronectin expressed specifically during wound healing (Singh et al., 2004). However, the identity of the keratinocyte α9β1 ligands under normal conditions was still unknown. Given our present finding that α9 represents a specific integrin receptor for EMILIN1 in keratinocytes and to reconcile the different results obtained in *Emilin1*$^{-/-}$ compared with K14-α9–null mice, it is tempting to speculate that EMILIN1 might represent the α9-specific ligand of normal skin.

A model summarizing how EMILIN1-occupied α4β1 and/or α9β1 integrins maintained homeostatic proliferative cues in basal keratinocytes and dermis fibroblasts is shown in Fig. 9. Consistent with this proposed role, we suggest that the extrinsic signals couple with the intrinsic properties (i.e., stemness?) of

the basal epidermal cells to define their ability to self-renew. The novel ligand–receptor pair (i.e., EMILIN1-α9β1) supported a scenario in which one of the functional consequences is the integration of EMILIN1 into the complex connections of basal keratinocyte turnover and the cross talks between basal keratinocytes, underlying ECM, and stromal cells. Whereas signals generated by ligand-activated integrins are in general proproliferative (Clark and Brugge, 1995; Walker and Assoian, 2005; Gilcrease, 2007; Streuli, 2009), signals emanating from EMILIN1-ligated α4/α9 integrins were antiproliferative. It has been suggested that proliferation and antiproliferation signals occur simultaneously within the same cell, and the antiproliferative effectors accumulate over time (EMILIN1 ligation in the present model) and override the proproliferative signals when they reach a certain threshold (Müller et al., 2008). This study unveiled another piece of the complex puzzle of skin homeostasis and opened new perspectives in the molecular mechanisms of basal keratinocytes quiescence.

Materials and methods

Antibodies and other reagents

Rat monoclonal anti–mouse EMILIN1 (clone 1007C11A8) and mouse anti–human gC1q (clone 1H2) antibodies were produced in our laboratories as previously described (Spessotto et al., 2003; Danussi et al., 2008). Rabbit anti–Keratin 5 (AF 138), Keratin 1 (AF 109), and loricrin (AF 62) antibodies were purchased from Covance. Rabbit antioccludin and ZO-1 were obtained from Invitrogen. Rabbit anti–β-catenin, anti–phospho-p44/42 MAPK (Erk1/2; Thr202/Tyr204), anti–phospho-Smad2 (C-terminal Ser465/467 and linker region Ser245/250/255), anti-Smad2/3, anti–phospho-Akt (Thr308 and Ser 473), anti-Akt, anti-PTEN, and anti–PI3K p110-α antibodies were obtained from Cell Signaling Technology. Goat anti-Erk1/2 and rabbit anti-p27, rabbit anti–Cyclin A, and goat antivinculin antibodies were obtained from Santa Cruz Biotechnology, Inc. Rabbit anti-Ki67, Keratin 6, laminin-5, collagen IV, and entactin/nidogen antibodies were purchased from Abcam. Moreover, mouse anti-CdK2 (BD), mouse anti–Cyclin D1/2 (Millipore), rabbit anti–mature TGF-β1 (BioVision Research Products), rabbit anti–pan-CK antibody (Dako), mouse anti–integrin α9β1 (clone Y9A2) and anti–integrin α4 (clone P1H4; Millipore), goat anti–mouse integrin α9β1 (LifeSpan BioSciences), and mouse anti–β1 integrin subunit (clone 4B4; Beckman Coulter) antibodies were used.

The C-terminal domain of EMILIN1 (gC1q) and the recombinant mutants of the integrin-binding sequence of gC1q were produced as previously described (Fig. S3; Spessotto et al., 2003; Verdone et al., 2008) and were provided by R. Doliana and A. Capuano (Centro di Riferimento Oncologico National Cancer Institute, Aviano, Italy). Recombinant human TGF-β1 was purchased from PeproTech EC.

Mice

Procedures involving animals and their care were conducted according to the institutional guidelines in compliance with national laws (Legislative decree no. 116/92). WT and *Emilin1*$^{-/-}$ mice (CD1 strain) were generated as previously described by Zanetti et al. (2004). *Emilin1*$^{+/+}$*TGF-β*$^{+/+}$, *Emilin1*$^{+/+}$*TGF-β*$^{+/-}$, *Emilin1*$^{-/-}$*TGF-β*$^{+/+}$, and *Emilin1*$^{-/-}$*TGF-β*$^{+/-}$ were obtained crossing WT and *Emilin1*$^{-/-}$ mice with *TGF-β*$^{+/-}$ mice, which were provided by G.M. Bressan (University of Padua, Padova, Italy). Genotypes were determined by PCR screening of tail biopsies (Maxwell mouse tail DNA purification kit; Promega).

Cells and culture procedures

Keratinocytes, HFs, and fibroblasts were isolated from WT and *Emilin1*$^{-/-}$ newborn mice (1–3 d old) as described by Lichti et al. (2008) and cultured, respectively, in KGM-2 medium (Cambrex Corporation) plus 0.05 mM $CaCl_2$ and in DME (Lonza) supplemented with 10% FCS. NIH 3T3 (mouse fibroblasts), HT1080 (fibrosarcoma), RD, HeLa (cervix adenocarcinoma), and CaCo-2 (colorectal adenocarcinoma) cell lines were purchased from American Type Culture Collection and cultured in DME supplemented with 10% FCS. The HaCaT (immortalized human keratinocytes) cell line was provided by L. Banks (International Centre for Genetic Engineering and Biotechnology, Italy) and cultured in DME supplemented with 10% FCS.

Histological and immunofluorescence analysis

Mouse dorsal skin specimens were excised and processed, embedded in optimal cutting temperature compound (Kaltek), snap frozen, and stored at −80°C. Cryostat sections of 7 µm were air dried at room temperature and kept at −80°C wrapped in aluminum foil. For histological analysis, sections were stained with hematoxylin/eosin (H/E). For immunofluorescence staining, the sections were equilibrated at room temperature, hydrated with PBS for 5 min, and fixed with PBS 4% PFA for 15 min. Then, they were permeabilized (with PBS, 1% BSA, 0.1% Triton X-100, and 2% FCS) for 5 min and saturated with the blocking buffer (PBS, 1% BSA, and 2% FCS) for 30 min. The primary antibodies were then incubated at room temperature for 1 h followed by three 5-min washes in PBS, and the secondary antibody incubation was performed for 1 h. Multiple staining was performed using a combination of different secondary antibodies conjugated with Alexa Fluor 488 and 568 (Invitrogen). Nuclei were visualized with TO-PRO (Invitrogen). Images were acquired with a true confocal scanner system (SP2; Leica) equipped with an HC PL Fluotar 10×/0.30 NA and HCX PL Apo 40×/1.25–0.75 NA and HCX PL Apo 63×/1.40–0.60 NA oil objectives (Leica) using Leica confocal software.

BrdU proliferation assay

Cells were grown on glass coverslips at defined times and conditions. Then, the incorporation of BrdU was performed using the BrdU labeling and detection kit (Roche) according to the manufacturer's instructions. The proliferation index was expressed as a percentage of the mean number of BrdU-positive cells per field (63× magnification).

Cell adhesion assay

The quantitative cell adhesion assay used in this study is based on centrifugation and has been previously described (Spessotto et al., 2009). 6-well strips of flexible polyvinyl chloride–denoted centrifugal assay for fluorescence-based cell adhesion (CAFCA) miniplates covered with double-sided tape (bottom units) were coated with 20 µg/ml gC1q. Cells were labeled with the vital fluorochrome calcein acetoxymethyl (Invitrogen) for 15 min at 37°C and were then aliquoted into the bottom CAFCA miniplates, which were centrifuged to synchronize the contact of the cells with the substrate. The miniplates were then incubated for 20 min at 37°C and were subsequently mounted together with a similar CAFCA miniplate to create communicating chambers for subsequent reverse centrifugation. The relative number of cells bound to the substrate (i.e., remaining in the wells of the bottom miniplates) and cells that failed to bind to the substrate (i.e., remaining in the wells of the top miniplates) was estimated by top/bottom fluorescence detection in a computer-interfaced GENios Plus microplate reader (Tecan Group Ltd.).

Impedance measurement with the XCELLigence system

To quantitatively monitor cell behavior in real time, we adopted the innovative technology provided by the Real-Time Cell Analyzer dual plate instrument (Roche). The strategy is based on continuous quantitative monitoring of cells as they adhere and proliferate by measuring electrical impedance (Xing et al., 2005). The change in impedance caused by cell attachment and proliferation is expressed as the cell index, which is an arbitrary measurement defined as $(R_n - R_b)/15$, in which R_b is the background impedance of the well measured with medium alone, and R_n is the impedance of the well measured at any time (t) with cells present. Thus, the cell index is a reflection of overall cell number, attachment quality, and cell morphology that can change as a function of time. The Real-Time Cell Analyzer dual plate instrument was placed in a humidified incubator maintained at 37°C with 95% air/5% CO_2. For adhesion experiments, the E-plates 96 were precoated with the gC1q domain or its mutants (20 µg/ml), and cells were then seeded at 40,000 cells/well in FCS-free medium. Cells were monitored once every 5 min for 2 h. For proliferation, cells were seeded in E-plates 96 at 20,000 cells/well in FCS-containing medium and in the presence or in the absence of the gC1q domain or its mutants (5 µg/ml) The E-plates 96 were monitored every 30 min for 48 h. Data analysis was performed using Real-Time Cell Analyzer software (version 1.2) supplied with the instrument.

Western blotting

Shaved dorsal skin samples were collected from 6–8-wk-old WT and *Emilin1*$^{-/-}$ mice. In brief, the skin was flash frozen with dry ice, and the epidermis was removed by scraping it off with a cold scalpel. Tissue extracts were prepared in tissue protein extraction reagent lysis buffer supplemented with

protease inhibitor cocktail (both obtained from Thermo Fisher Scientific). The protein content of the samples was determined using Bradford protein assay reagent (Bio-Rad Laboratories), and Western blot analysis was performed as previously described (Spessotto et al., 2006). Signal quantification was performed by Quantity One software (Bio-Rad Laboratories).

RNA extraction and RT-PCR

Total cellular RNA was isolated from mouse keratinocytes, HFs, and dermal fibroblasts using TRIZOL (Invitrogen) according to the manufacturer's protocol. Reverse transcription reactions were performed with 1 µg of total RNA using Avian Myeloblastosis Virus reverse transcription (Promega). RNA was reverse transcribed into first-strand cDNA using random hexamer primers. The primers used for the PCR amplification of mouse EMILIN1 were 5′-TGTGCCTAGGGTAGCATTTTC-3′ and 5′-GAGGCTGAAGACGCCCAGAG-3′. The size of the amplification product was 320 bp. Taq DNA polymerase was obtained from Roche. RT-PCR amplification of a 700-bp fragment of β-actin cDNA served as a positive internal control. Amplification products were resolved on 2% agarose gels stained with ethidium bromide.

Computer-assisted morphometric analyses

Images of H/E-stained skin cryostat sections were captured with a camera (ICC50; Leica) connected with a microscope (DM 750; Leica) equipped with an N Plan objective 5×/−0.12 NA and HI-Plan objective 10×/0.25 NA and objective 20× (Leica). The thickness of mouse skin layers was then evaluated by ImageJ (NIH) computer-assisted morphometric analysis. To quantitatively evaluate the proliferation index of mouse skin, cryostat sections were stained with an anti-Ki67 antibody. The images, acquired with a true confocal scanner system (SP2), were analyzed by ImageJ software, and the number of Ki67-positive cells was related to epidermis length (micrometers) and to the dermis area (micrometers squared).

EMILIN1 silencing

Mouse EMILIN1 expression was abrogated by stably transfecting NIH 3T3 fibroblasts with HuSH-29 pRS plasmids (OriGene Technologies, Inc.). Among the provided vectors, the most effective shRNA construct presented the following sequence: 5′-GAGTCTGCGAACGACTGGACACCGTGGCA-3′. Negative controls included scrambled noneffective shRNA. The transfection of NIH 3T3 cells was performed according to the manufacturer's instructions. The stable clones were selected and maintained in complete medium supplemented with 1 µg/ml puromycin.

PTEN silencing

PTEN-silenced CaCo-2 and HaCaT cells were generated using three shRNAs against human PTEN from the MISSION library (TRCN0000002746, TRCN0000002747, and TRCN0000002749; the underlined bold text indicates clone numbers in the Results section; Sigma-Aldrich) using stable (puromycin selected) lentiviral transduction with no significant differences among the shRNAs used. The nontarget sh-control vector (SHC202; Sigma-Aldrich) was used as a negative control.

Flow cytometry

The expression of integrins on the cell surface was analyzed by single-color indirect immunofluorescence. Isotype-matched control mAbs and phycoerythrin-conjugated $F(ab)^2$ fragments of goat anti–mouse Igs (Jackson ImmunoResearch Laboratories, Inc.) were used. Viable antibody-labeled cells were identified according to their forward and side scatter, electronically gated, and assayed for surface fluorescence on a FACScan flow cytometer (BD).

Cutaneous wound healing assay

To generate excisional wounds, 7-wk-old mice were anesthetized, and the dorsal skin was shaved. After sanitizing with 70% ethanol, two full-thickness wounds were generated on the dorsal skin using 4-mm-diameter dermal biopsy punches (Integra LifeSciences Corporation). The size of the closing wound was monitored daily until day 7. The percentage of wound closure was calculated as the ratio of the remaining open wound over the original wound size.

Statistical analysis

Statistical significance of the results was determined by using the unpaired and paired Student's *t* test. A value of $P < 0.05$ was considered significant.

Online supplemental material

Fig. S1 shows skin hyperplastic phenotype in *Emilin1*$^{-/-}$ mouse embryos. Fig. S2 shows the comparable expression of basal membrane/ECM, polarity and cell junctional markers, and normal barrier function of WT and *Emilin1*$^{-/-}$ mouse skin. Fig.S3 shows gC1q mutants and their binding activity. Fig. S4 shows that EMILIN1 deficiency overrides the TGF-β effect on epidermal and dermal proliferation. Online supplemental material is available at http://www.jcb.org/cgi/content/full/jcb.201008013/DC1.

The authors thank Drs. Roberto Doliana and Alessandra Capuano for providing gC1q mutants and Drs. Donatella Aldinucci and Marta Celegato for their excellent assistance in flow cytometry.

This work was supported by grants to P. Spessotto from the Associazione Italiana per la Ricerca sul Cancro (IG 10119), to A. Colombatti from the Associazione Italiana per la Ricerca sul Cancro (ACC2 WP5/5), Programmi di ricerca di Rilevante Interesse Nazionale (20074S758W_002), and Fondo Investimenti in Ricerca di Base (RBRN07BMCT). C. Danussi is a recipient of a Federazione Italiana Ricerca sul Cancro fellowship.

No conflict of interest regarding sources of financial support, corporate involvement, patent holding, etc. has to be disclosed for the present study.

Submitted: 2 August 2010
Accepted: 6 September 2011

References

Annes, J.P., J.S. Munger, and D.B. Rifkin. 2003. Making sense of latent TGFbeta activation. *J. Cell Sci.* 116:217–224. http://dx.doi.org/10.1242/jcs.00229

Beck, S., J.A. Le Good, M. Guzman, N. Ben Haim, K. Roy, F. Beermann, and D.B. Constam. 2002. Extraembryonic proteases regulate Nodal signalling during gastrulation. *Nat. Cell Biol.* 4:981–985. http://dx.doi.org/10.1038/ncb890

Blanpain, C., and E. Fuchs. 2009. Epidermal homeostasis: a balancing act of stem cells in the skin. *Nat. Rev. Mol. Cell Biol.* 10:207–217. http://dx.doi.org/10.1038/nrm2636

Böck, P. 1983. Elastic fiber microfibrils: filaments that anchor the epithelium of the epiglottis. *Arch. Histol. Jpn.* 46:307–314. http://dx.doi.org/10.1679/aohc.46.307

Böttinger, E.P., J.L. Jakubczak, I.S. Roberts, M. Mumy, P. Hemmati, K. Bagnall, G. Merlino, and L.M. Wakefield. 1997. Expression of a dominant-negative mutant TGF-beta type II receptor in transgenic mice reveals essential roles for TGF-beta in regulation of growth and differentiation in the exocrine pancreas. *EMBO J.* 16:2621–2633. http://dx.doi.org/10.1093/emboj/16.10.2621

Bressan, G.M., D. Daga-Gordini, A. Colombatti, I. Castellani, V. Marigo, and D. Volpin. 1993. Emilin, a component of elastic fibers preferentially located at the elastin-microfibrils interface. *J. Cell Biol.* 121:201–212. http://dx.doi.org/10.1083/jcb.121.1.201

Chow, J.Y., J.A. Cabral, J. Chang, and J.M. Carethers. 2008. TGFbeta modulates PTEN expression independently of SMAD signaling for growth proliferation in colon cancer cells. *Cancer Biol. Ther.* 7:1694–1699. http://dx.doi.org/10.4161/cbt.7.10.6665

Clark, E.A., and J.S. Brugge. 1995. Integrins and signal transduction pathways: the road taken. *Science*. 268:233–239. http://dx.doi.org/10.1126/science.7716514

Clayton, E., D.P. Doupé, A.M. Klein, D.J. Winton, B.D. Simons, and P.H. Jones. 2007. A single type of progenitor cell maintains normal epidermis. *Nature*. 446:185–189. http://dx.doi.org/10.1038/nature05574

Colombatti, A., G.M. Bressan, I. Castellani, and D. Volpin. 1985. Glycoprotein 115, a glycoprotein isolated from chick blood vessels, is widely distributed in connective tissue. *J. Cell Biol.* 100:18–26. http://dx.doi.org/10.1083/jcb.100.1.18

Colombatti, A., R. Doliana, S. Bot, A. Canton, M. Mongiat, G. Mungiguerra, S. Paron-Cilli, and P. Spessotto. 2000. The EMILIN protein family. *Matrix Biol.* 19:289–301. http://dx.doi.org/10.1016/S0945-053X(00)00074-3

Danussi, C., P. Spessotto, A. Petrucco, B. Wassermann, P. Sabatelli, M. Montesi, R. Doliana, G.M. Bressan, and A. Colombatti. 2008. Emilin1 deficiency causes structural and functional defects of lymphatic vasculature. *Mol. Cell. Biol.* 28:4026–4039. http://dx.doi.org/10.1128/MCB.02062-07

Doliana, R., M. Mongiat, F. Bucciotti, E. Giacomello, R. Deutzmann, D. Volpin, G.M. Bressan, and A. Colombatti. 1999. EMILIN, a component of the elastic fiber and a new member of the C1q/tumor necrosis factor superfamily of proteins. *J. Biol. Chem.* 274:16773–16781. http://dx.doi.org/10.1074/jbc.274.24.16773

Doliana, R., S. Bot, P. Bonaldo, and A. Colombatti. 2000. EMI, a novel cysteine-rich domain of EMILINs and other extracellular proteins, interacts with the gC1q domains and participates in multimerization. *FEBS Lett.* 484:164–168. http://dx.doi.org/10.1016/S0014-5793(00)02140-2

Ebert, M.P., G. Fei, L. Schandl, C. Mawrin, K. Dietzmann, P. Herrera, H. Friess, T.M. Gress, and P. Malfertheiner. 2002. Reduced PTEN expression in the

pancreas overexpressing transforming growth factor-beta 1. *Br. J. Cancer*. 86:257–262. http://dx.doi.org/10.1038/sj.bjc.6600031

Fuchs, E. 2007. Scratching the surface of skin development. *Nature*. 445:834–842. http://dx.doi.org/10.1038/nature05659

Fuchs, E., and S. Raghavan. 2002. Getting under the skin of epidermal morphogenesis. *Nat. Rev. Genet.* 3:199–209. http://dx.doi.org/10.1038/nrg758

Gilcrease, M.Z. 2007. Integrin signaling in epithelial cells. *Cancer Lett.* 247:1–25. http://dx.doi.org/10.1016/j.canlet.2006.03.031

Grose, R., V. Fantl, S. Werner, A.M. Chioni, M. Jarosz, R. Rudling, B. Cross, I.R. Hart, and C. Dickson. 2007. The role of fibroblast growth factor receptor 2b in skin homeostasis and cancer development. *EMBO J.* 26:1268–1278. http://dx.doi.org/10.1038/sj.emboj.7601583

Hamajima, H., I. Ozaki, H. Zhang, S. Iwane, Y. Kawaguchi, Y. Eguchi, S. Matsuhashi, T. Mizuta, K. Matsuzaki, and K. Fujimoto. 2009. Modulation of the transforming growth factor-beta1-induced Smad phosphorylation by the extracellular matrix receptor beta1-integrin. *Int. J. Oncol.* 35:1441–1447.

Kikkawa, Y., N. Sanzen, and K. Sekiguchi. 1998. Isolation and characterization of laminin-10/11 secreted by human lung carcinoma cells. laminin-10/11 mediates cell adhesion through integrin alpha3 beta1. *J. Biol. Chem.* 273: 15854–15859. http://dx.doi.org/10.1074/jbc.273.25.15854

Kikkawa, Y., N. Sanzen, H. Fujiwara, A. Sonnenberg, and K. Sekiguchi. 2000. Integrin binding specificity of laminin-10/11: laminin-10/11 are recognized by alpha 3 beta 1, alpha 6 beta 1 and alpha 6 beta 4 integrins. *J. Cell Sci.* 113:869–876.

Kretzschmar, M., J. Doody, I. Timokhina, and J. Massagué. 1999. A mechanism of repression of TGFbeta/ Smad signaling by oncogenic Ras. *Genes Dev.* 13:804–816. http://dx.doi.org/10.1101/gad.13.7.804

Li, D.M., and H. Sun. 1997. TEP1, encoded by a candidate tumor suppressor locus, is a novel protein tyrosine phosphatase regulated by transforming growth factor beta. *Cancer Res.* 57:2124–2129.

Liao, Y.F., P.J. Gotwals, V.E. Koteliansky, D. Sheppard, and L. Van De Water. 2002. The EIIIA segment of fibronectin is a ligand for integrins alpha 9beta 1 and alpha 4beta 1 providing a novel mechanism for regulating cell adhesion by alternative splicing. *J. Biol. Chem.* 277:14467–14474. http://dx.doi.org/10.1074/jbc.M201100200

Lichti, U., J. Anders, and S.H. Yuspa. 2008. Isolation and short-term culture of primary keratinocytes, hair follicle populations and dermal cells from newborn mice and keratinocytes from adult mice for in vitro analysis and for grafting to immunodeficient mice. *Nat. Protoc.* 3:799–810. http://dx.doi.org/10.1038/nprot.2008.50

Marinkovich, M.P., P. Verrando, D.R. Keene, G. Meneguzzi, G.P. Lunstrum, J.P. Ortonne, and R.E. Burgeson. 1993. Basement membrane proteins kalinin and nicein are structurally and immunologically identical. *Lab. Invest.* 69:295–299.

Masunaga, T., H. Shimizu, C. Yee, L. Borradori, Z. Lazarova, T. Nishikawa, and K.B. Yancey. 1997. The extracellular domain of BPAG2 localizes to anchoring filaments and its carboxyl terminus extends to the lamina densa of normal human epidermal basement membrane. *J. Invest. Dermatol.* 109:200–206. http://dx.doi.org/10.1111/1523-1747.ep12319337

Mongiat, M., G. Mungiguerra, S. Bot, M.T. Mucignat, E. Giacomello, R. Doliana, and A. Colombatti. 2000. Self-assembly and supramolecular organization of EMILIN. *J. Biol. Chem.* 275:25471–25480. http://dx.doi.org/10.1074/jbc.M001426200

Müller, E.J., L. Williamson, C. Kolly, and M.M. Suter. 2008. Outside-in signaling through integrins and cadherins: a central mechanism to control epidermal growth and differentiation? *J. Invest. Dermatol.* 128:501–516. http://dx.doi.org/10.1038/sj.jid.5701248

Nishiyama, T., S. Amano, M. Tsunenaga, K. Kadoya, A. Takeda, E. Adachi, and R.E. Burgeson. 2000. The importance of laminin 5 in the dermal-epidermal basement membrane. *J. Dermatol. Sci.* 24(Suppl 1):S51–S59. http://dx.doi.org/10.1016/S0923-1811(00)00142-0

Owens, D.M., and F.M. Watt. 2003. Contribution of stem cells and differentiated cells to epidermal tumours. *Nat. Rev. Cancer*. 3:444–451. http://dx.doi.org/10.1038/nrc1096

Palmer, E.L., C. Rüegg, R. Ferrando, R. Pytela, and D. Sheppard. 1993. Sequence and tissue distribution of the integrin alpha 9 subunit, a novel partner of beta 1 that is widely distributed in epithelia and muscle. *J. Cell Biol.* 123:1289–1297. http://dx.doi.org/10.1083/jcb.123.5.1289

Schwartz, M.A., M.D. Schaller, and M.H. Ginsberg. 1995. Integrins: emerging paradigms of signal transduction. *Annu. Rev. Cell Dev. Biol.* 11:549–599. http://dx.doi.org/10.1146/annurev.cb.11.110195.003001

Shinde, A.V., C. Bystroff, C. Wang, M.G. Vogelezang, P.A. Vincent, R.O. Hynes, and L. Van De Water. 2008. Identification of the peptide sequences within the EIIIA (EDA) segment of fibronectin that mediate integrin alpha9beta1-dependent cellular activities. *J. Biol. Chem.* 283:2858–2870. http://dx.doi.org/10.1074/jbc.M708306200

Singer, A.J., and R.A. Clark. 1999. Cutaneous wound healing. *N. Engl. J. Med.* 341:738–746. http://dx.doi.org/10.1056/NEJM199909023411006

Singh, P., C.L. Reimer, J.H. Peters, M.A. Stepp, R.O. Hynes, and L. Van De Water. 2004. The spatial and temporal expression patterns of integrin alpha9beta1 and one of its ligands, the EIIIA segment of fibronectin, in cutaneous wound healing. *J. Invest. Dermatol.* 123:1176–1181. http://dx.doi.org/10.1111/j.0022-202X.2004.23485.x

Singh, P., C. Chen, S. Pal-Ghosh, M.A. Stepp, D. Sheppard, and L. Van De Water. 2009. Loss of integrin alpha9beta1 results in defects in proliferation, causing poor re-epithelialization during cutaneous wound healing. *J. Invest. Dermatol.* 129:217–228. http://dx.doi.org/10.1038/jid.2008.201

Spessotto, P., M. Cervi, M.T. Mucignat, G. Mungiguerra, I. Sartoretto, R. Doliana, and A. Colombatti. 2003. beta 1 Integrin-dependent cell adhesion to EMILIN-1 is mediated by the gC1q domain. *J. Biol. Chem.* 278:6160–6167. http://dx.doi.org/10.1074/jbc.M208322200

Spessotto, P., R. Bulla, C. Danussi, O. Radillo, M. Cervi, G. Monami, F. Bossi, F. Tedesco, R. Doliana, and A. Colombatti. 2006. EMILIN1 represents a major stromal element determining human trophoblast invasion of the uterine wall. *J. Cell Sci.* 119:4574–4584. http://dx.doi.org/10.1242/jcs.03232

Spessotto, P., K. Lacrima, P.A. Nicolosi, E. Pivetta, M. Scapolan, and R. Perris. 2009. Fluorescence-based assays for in vitro analysis of cell adhesion and migration. *Methods Mol. Biol.* 522:221–250. http://dx.doi.org/10.1007/978-1-59745-413-1_16

Stepp, M.A., H.E. Gibson, P.H. Gala, D.D. Iglesia, A. Pajoohesh-Ganji, S. Pal-Ghosh, M. Brown, C. Aquino, A.M. Schwartz, O. Goldberger, et al. 2002. Defects in keratinocyte activation during wound healing in the syndecan-1-deficient mouse. *J. Cell Sci.* 115:4517–4531. http://dx.doi.org/10.1242/jcs.00128

Streuli, C.H. 2009. Integrins and cell-fate determination. *J. Cell Sci.* 122:171–177. http://dx.doi.org/10.1242/jcs.018945

Tang, B., E.P. Böttinger, S.B. Jakowlew, K.M. Bagnall, J. Mariano, M.R. Anver, J.J. Letterio, and L.M. Wakefield. 1998. Transforming growth factor-beta1 is a new form of tumor suppressor with true haploid insufficiency. *Nat. Med.* 4:802–807. http://dx.doi.org/10.1038/nm0798-802

Tang, B., K. de Castro, H.E. Barnes, W.T. Parks, L. Stewart, E.P. Böttinger, D. Danielpour, and L.M. Wakefield. 1999. Loss of responsiveness to transforming growth factor beta induces malignant transformation of nontumorigenic rat prostate epithelial cells. *Cancer Res.* 59:4834–4842.

Verdone, G., R. Doliana, A. Corazza, S.A. Colebrooke, P. Spessotto, S. Bot, F. Bucciotti, A. Capuano, A. Silvestri, P. Viglino, et al. 2008. The solution structure of EMILIN1 globular C1q domain reveals a disordered insertion necessary for interaction with the alpha4beta1 integrin. *J. Biol. Chem.* 283:18947–18956. http://dx.doi.org/10.1074/jbc.M801085200

Walker, J.L., and R.K. Assoian. 2005. Integrin-dependent signal transduction regulating cyclin D1 expression and G1 phase cell cycle progression. *Cancer Metastasis Rev.* 24:383–393. http://dx.doi.org/10.1007/s10555-005-5130-7

Watt, F.M. 2002. Role of integrins in regulating epidermal adhesion, growth and differentiation. *EMBO J.* 21:3919–3926. http://dx.doi.org/10.1093/emboj/cdf399

White, E.S., V.J. Thannickal, S.L. Carskadon, E.G. Dickie, D.L. Livant, S. Markwart, G.B. Toews, and D.A. Arenberg. 2003. Integrin $\alpha4\beta1$ regulates migration across basement membranes by lung fibroblasts: a role for phosphatase and tensin homologue deleted on chromosome 10. *Am. J. Respir. Crit. Care Med.* 168:436–442. http://dx.doi.org/10.1164/rccm.200301-041OC

Xing, J.Z., L. Zhu, J.A. Jackson, S. Gabos, X.J. Sun, X.B. Wang, and X. Xu. 2005. Dynamic monitoring of cytotoxicity on microelectronic sensors. *Chem. Res. Toxicol.* 18:154–161. http://dx.doi.org/10.1021/tx049721s

Yokosaki, Y., E.L. Palmer, A.L. Prieto, K.L. Crossin, M.A. Bourdon, R. Pytela, and D. Sheppard. 1994. The integrin alpha 9 beta 1 mediates cell attachment to a non-RGD site in the third fibronectin type III repeat of tenascin. *J. Biol. Chem.* 269:26691–26696.

Yokosaki, Y., H. Monis, J. Chen, and D. Sheppard. 1996. Differential effects of the integrins alpha9beta1, alphavbeta3, and alphavbeta6 on cell proliferative responses to tenascin. Roles of the beta subunit extracellular and cytoplasmic domains. *J. Biol. Chem.* 271:24144–24150. http://dx.doi.org/10.1074/jbc.271.39.24144

Zacchigna, L., C. Vecchione, A. Notte, M. Cordenonsi, S. Dupont, S. Maretto, G. Cifelli, A. Ferrari, A. Maffei, C. Fabbro, et al. 2006. Emilin1 links TGF-beta maturation to blood pressure homeostasis. *Cell*. 124:929–942. http://dx.doi.org/10.1016/j.cell.2005.12.035

Zanetti, M., P. Braghetta, P. Sabatelli, I. Mura, R. Doliana, A. Colombatti, D. Volpin, P. Bonaldo, and G.M. Bressan. 2004. EMILIN-1 deficiency induces elastogenesis and vascular cell defects. *Mol. Cell. Biol.* 24:638–650. http://dx.doi.org/10.1128/MCB.24.2.638-650.2004

Zhang, Y.E. 2009. Non-Smad pathways in TGF-beta signaling. *Cell Res.* 19:128–139. http://dx.doi.org/10.1038/cr.2008.328